Battery Equalization Using Bi-directional Cûk Converters in DCVM Operation

Yuang-Shung Lee Chun-Yi Duh
Department of Electronic Engineering
Fu Jen Catholic University
Taiwan, R.O.C.
e-mail: lee@ee.fju.edu.tw

Guo-Tian Chen Shen-Ching Yang
Department of Electronic Engineering
Fu Jen Catholic University
Taiwan, R.O.C.
e-mail: a9250502@st2.fju.edu.tw

Abstract–A systematic approach to the analysis and design of a bi-directional Cûk converter for the cell voltage balancing control of a series-connected battery string is presented in this paper. The proposed individual cell equalizers (ICE) are designed to operate at discontinuous-capacitor-voltage mode (DCVM) to achieve the zero-voltage turn-off switching (ZVS) for reducing the switching loss of the bi-directional DC/DC converters. Simulation and experimental results show that the proposed battery equalization scheme can not only enhance the bi-directional battery equalization performance, but also can reduce the switching loss during the equalization period. The switch power is significantly reduced by about 52.8% from MOSFETs and the equalization efficiency can be improved by 68~72% using the proposed DCVM ZVS battery equalizer under the specified cell equalization process.

I. INTRODUCTION

Because the voltage in a single battery cell is limited, battery cells connected in series are usually employed in many applications, such as electric vehicles (EV), hybrid electric vehicles (HEV), or telecom battery energy systems. Imbalanced cell voltage within a series string can be attributed to the differences in cell internal resistance, imbalanced state-of-charge (SOC) between cells, degradation and the ambient temperature gradients of the battery pack during charging and discharging. Voltage monitoring and current diversion equalization schemes and battery management systems (BMS) have been presented in the literature to prevent imbalances during charging and discharging in a series connected battery cells [1-3].

Integrated individual cell equalization schemes (ICE) for battery pack applications have been proposed to equalize battery strings [3-6]. The bidirectional battery equalization scheme has many advantages such as higher equalization efficiency for non-dissipative current diverters, and a modular design approach [3]. The disadvantage of this equalization scheme is that the stored energy in the inductor is transferred to the weaker cell only in the (1-D)T_s duty cycle. The equalization time and efficiency of this equalization scheme are therefore poor for practical battery equalization applications in a smart battery management system (SBMS) [6-11]. Battery equalization control should be implemented to restrict the charge-discharge current to the allowable cell limitations in the battery string. Cell balancing control is designed to obtain the maximum usable capacity from the battery string. However, battery string charging and discharging are limited by any single cell reaching its end-of-charge voltage and by low voltage threshold. Cell balancing algorithms search to efficiently remove energy from a strong cell and transfer that energy into a weak one until the cell voltage is equalized across all cells. This enables additional charging capacity for the entire battery string [4]. Complete cell voltage balancing is performed using a bi-directional dc-dc converter based on the Cûk converter [9, 11]. This unit can be designed to operate at the DICM or DCVM to obtain soft switching in MOSFET switches [11-14].

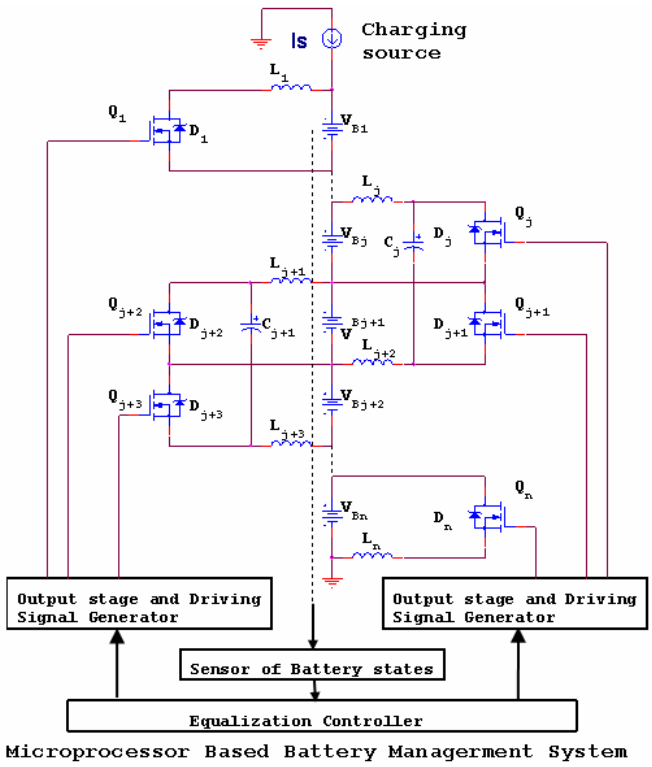

Fig. 1: Studied battery charging system with ICE and microprocessor based BMS

II. TOPOLOGY DESCRIPTIONS

The studied battery charging system with the proposed ICEs and the microprocessor based BMS is shown in fig. 1. The system is composed of N battery cells and (N-1) ICEs. The jth module is comprised of two inductors L_j and L_{j+1}, an energy transfer capacitor C_j, and two power MOSFETs with body diodes as the battery cell-balancing switches. The single module of ICE is redrawn and simplified in fig. 2. The cell voltage balancing control algorithm for this equalization

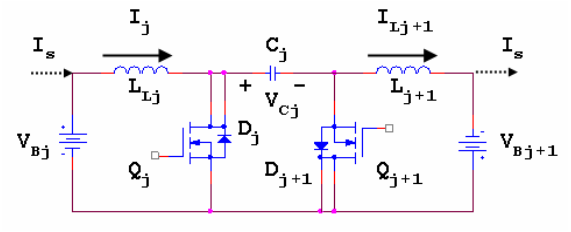

Fig. 2 Single stage of the proposed ICE

scheme is instructed by a microprocessor-based BMS. The energy between the adjoining battery cells is transformed through the energy transferring capacitor for cell voltage balancing. The energy transfer direction is determined by the cell voltage and/or SOC difference in the battery string and conduction from the controlled power MOSFET switches [9]. The two adjoining cells voltages are balanced by switching the MOSFETs on/off according to the PWM signals generated from the BMS. The PWM signals correspond to the respective cell voltage through the microprocessor-based BMS, which controls the switches Q_j and Q_{j+1}. The initial capacitor voltage V_{Cj} equals $V_{Bj}+V_{Bj+1}$. For example, the PWM control signal turns on/off the Q_j to transfer some of the stronger cell voltage, V_{Bj}, to the weak cell, V_{Bj+1}. The stronger cell energy is transferred from cell V_{Bj} to cell V_{Bj+1}. Conversely, if cell V_{Bj+1} is stronger than cell V_{Bj}, the energy is transferred from cell V_{Bj+1} to cell V_{Bj} by controlling the Q_{j+1}. The equalization process will be uninterrupted until the voltages in the remaining cells are all equalized to the same end-of-charge or end-of-discharge level. The proposed bidirectional battery equalizer is designed to operate at DCVM for achieving the zero voltage switching to reduce the MOSFETs switching losses. The DCVM operation principle of proposed ICE is described in the following section.

III. CIRCUIT ANALYSIS

The inductors L_1 and L_2 are assumed to be large enough to operate in CICM. In addition, the capacitor is also sufficiently small so it can be fully discharged during the switching period. Where T_s is the converter switching period, the detail equivalent circuit of the proposed battery equalization schemes are shown in figs. 3 and 4 during the various time intervals for the different cell voltage, $V_{Bj} > V_{Bj+1}$ and $V_{Bj} < V_{Bj+1}$, respectively. The corresponding typical switching waveforms for various operating states are depicted in figs. 5 (a) and 5 (b), respectively. Referring to the capacitor voltage waveform and the dynamic state equations of the ICE in fig. 5 (a) for $V_{Bj} > V_{Bj+1}$ can be explained as follows:

Assume the capacitor voltage υ_{cj} has reached a maximum before the main switch Q_j is turned on. From the duty cycle 0 to D_1T_s, the switch Q_j is turned on and diode D_{j+1} is turned off at the beginning of the switching cycle t = 0, as shown as fig. 3 (a). The inductor L_j is charged by input voltage V_{Bj} and the current i_{j+1} thought inductor L_{j+1} is discharged by capacitor C_j. The energy stored in C_j is completely transferred to the cell V_{Bj+1}, and υ_{cj} becomes to zero at $t = D_1T_s$. From the duty cycle D_1T_s to DT_s, the switch Q_{j+1} was still connected and D_{j+1} starts conducting to allow i_{j+1} to flow since υ_{cj} is equal to zero during this interval, as shown as fig. 3 (b), V_{Bj} continuous to charge

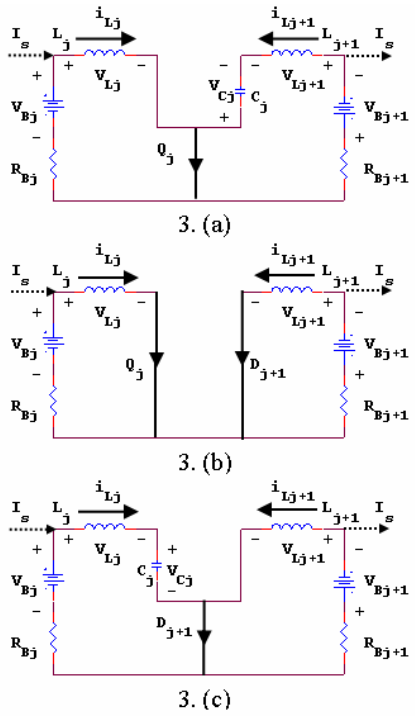

Fig. 3 Equivalent circuit of DCVM for $V_{Bj} > V_{Bj+1}$

(a) Q_j turn-on, (b) Q_j turn-on and $V_{Cj} = 0$, (c) Q_j turn-off and D_{j+1} turn-on

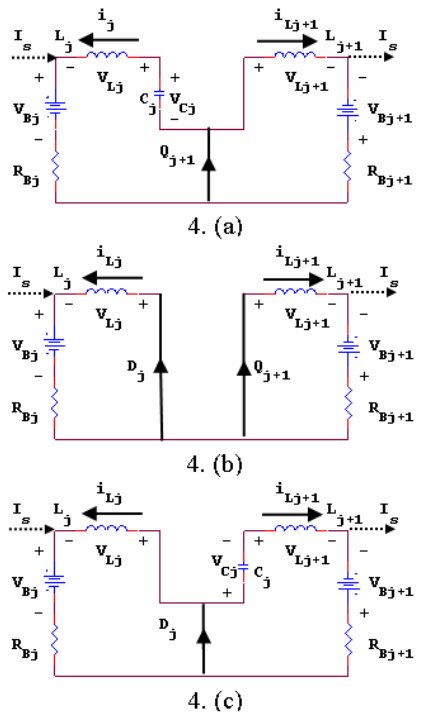

Fig. 4 Equivalent circuit of DCVM for $V_{Bj} < V_{Bj+1}$

(a) Q_{j+1} turn-on, (b) Q_{j+1} turn-on and V_{Cj} =0, (c) Q_{j+1} turn-off and D_j turn-on

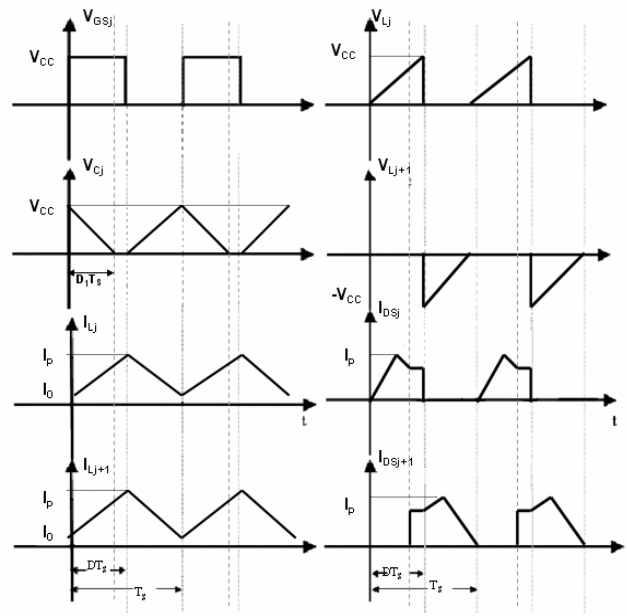

5. (a)

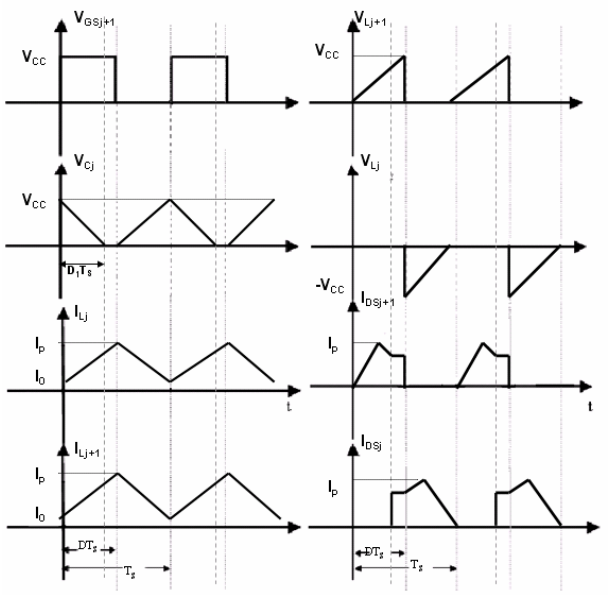

5. (b)

Fig. 5 Typical switching waveforms of ICE_j for (a) $V_{Bj}>V_{Bj+1}$, (b) $V_{Bj}<V_{Bj+1}$

L_j and the stored energy in L_{j+1} is still discharged to V_{Bj+1} for cell voltage balancing control. From duty cycle DT_s to T_s, the switch Q_j is turned off at $t = DT_s$, and D_{j+1} is still conducted for cell voltage balancing. Capacitor C_j is charged from zero voltage by i_j. The capacitor voltage υ_{cj} reaches maximum value at $t = T_s$, as shown in fig. 3 (c). The proposed ICE has more than one stage, in contrast with a Cûk converter in CICM, where both the MOSFET switch Q_j and flywheel diode D_{j+1} are conducting in the DCVM operation, as shown in fig. 3(b). The compact state equation for descriptions of the three states mentioned above can be derived as:

$$\begin{bmatrix} \frac{di_j}{dt} \\ \frac{di_{j+1}}{dt} \\ \frac{dV_C}{dt} \end{bmatrix} = \begin{bmatrix} -\frac{R_{B_j}}{L_j} & 0 & \frac{-(1-u)(\frac{1}{2}-u)\times 2}{L_j} \\ 0 & -\frac{R_{B_{j+1}}}{L_{j+1}} & \frac{2u(u-\frac{1}{2})}{L_{j+1}} \\ \frac{2(1-u)(\frac{1}{2}-u)}{C_j} & \frac{-2u(u-\frac{1}{2})}{C_j} & 0 \end{bmatrix} \begin{bmatrix} i_j \\ i_{j+1} \\ V_C \end{bmatrix} + \begin{bmatrix} \frac{V_{B_j}+I_s R_{B_j}}{L_j} \\ -\frac{V_{B_{j+1}}+I_s R_{B_{j+1}}}{L_{j+1}} \\ 0 \end{bmatrix} \tag{1}$$

where u is a tri-state switching control variable. It is also suggested that u = 1 (HIGH state) denotes Q_j turn-on and D_{j+1} turned off shown as fig. 3 (a), u = 0 (LOW state) denotes Q_j is turned off and D_{j+1} is turned on shown as fig. 3 (c), and u = 0.5 (FLOATING state) denotes Q_j and D_{j+1} are both turned on and $\upsilon_{cj} = 0$ shown as fig. 3 (b). The internal resistance of battery cell R_B is neglected to simplify the steady state circuit analysis, and the charging/discharging source effect is absent in the principle operation of the converter.

If L_j and L_{j+1} are enough large, the ripples in i_j and i_{j+1} are small. Denote the time average value of i_j and i_{j+1} as I_j and I_{j+1}, respectively. From fig. 5(a), we can derive the conditions of DCVM operation as follows:

The instantaneous capacitor voltage in the full duty cycle of the DCVM Cûk converter can be expressed as:

$$v_{Cj} = \begin{cases} \frac{I_j(1-D)T_S - I_{j+1}t}{C_j}, & \text{for } 0 < t < D_1T_S \\ 0, & \text{for } D_1T_S < t < DT_S \\ \frac{I_j(t-DT_S)}{C_j}, & \text{for } DT_S < t < T_S \end{cases} \tag{2}$$

The power MOSFETs of the modified QRZVS battery equalizer are turned off at the zero current. The sub-duty ratio D_1 in terms of the duty ratio D can be governed as:

$$D_1 = (1 - D)\frac{I_j}{I_{j+1}} \tag{3}$$

The time-average of voltages of υ_{cj} and υ_{Dj+1} are denoted as V_{cj} and V_{Dj+1}, respectively. This can be determined from (2) as

$$V_{cj} = \frac{T_s}{2C_j} I_j (1 - D)(1 - D + D_1) \tag{4}$$

$$V_{Dj+1} = -\frac{T_s}{2C_j} I_j (1 - D) D_1 \tag{5}$$

Therefore, the terminal voltages of the battery cells and the voltage conversion ratio are

$$V_{Bj+1} = -V_{Dj+1} = \frac{T_s}{2C_j} I_j (1 - D) D_1 \tag{6}$$

$$V_{Bj} = V_{Dj+1} + V_{Cj} = \frac{Ts}{2C_j} I_j (1 - D)^2 \quad (7)$$

$$\frac{V_{Bj+1}}{V_{Bj}} = \frac{D_1}{1 - D} \quad (8)$$

Combining (3) and (6) and substituting into (8) to yield

$$I_j = \frac{2 f_S C_j V_{Bj}}{(1 - D)^2} \quad (9)$$

$$D_1 = \sqrt{2 f_S C_j \frac{V_{Bj+1}}{I_{j+1}}} \quad (10)$$

To operate the proposed ICE in DCVM, the inequality should be satisfied, or equivalent

$$D \geq \sqrt{2 f_S C_j \frac{V_{Bj+1}}{I_{j+1}}} \quad (11)$$

$$L_j \geq \frac{V_{Bj+1}(1 - D)^2}{2 D f_S I_{j+1}} \quad (12)$$

$$L_{j+1} \geq \frac{V_{Bj+1}(1 - D)}{2 f_S I_{j+1}} \quad (13)$$

The switching boundary surface of the converter to operate between DCVM and continuous-capacitor-voltage mode (CCVM) is depicted in fig. 6. However, the proposed converter may not operate in DCVM when V_{Bj} is small because the cell voltages do not have constant dc voltage and depending on the equalization current of ICE. The inequalities (11), (12) and (13) are used to design the proposed ICE that can be guaranteed to operate in DCVM [10].

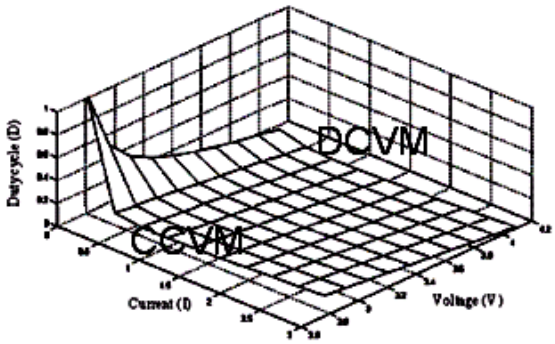

Fig. 6 Switching boundary surface between DCVM and CCVM

IV. SIMULATION AND EXPERIMENT RESULTS

In order to validate the performance of the proposed bi-directional battery equalizer, a Matlab/Simulink simulation and an experiment were carried out for a three- cell battery modular (N=3) with the two proposed battery equalizers (2ICEs). Matlab/Simulink simulation was performed for mathematical model of ICEs. A three-modular battery stack with two fundamental equalization schemes was used to verify the analysis results mentioned above. The simple signal flow graph is defined using Matlab/Simulink simulation for the proposed ICE Matlab/Simulink model for a three battery-cell. The ICE_1 (composed of L_1, L_2, C_1, Q_1 and Q_2) and the ICE_2 (composed of L_3, L_4, C_2, Q_3 and Q_4) comprise the block diagram shown in fig. 7. The battery storage elements were simply assumed for the battery charge/discharge model, which was established by a battery charge/discharge profile with equivalent series resistor (ESR) in the library of the Matlab/simulink block model. The battery initial voltages, inductors and energy transferring capacitor with ESR were set as V_{B1}=4.0(V), V_{B2}=3.9(V), V_{B3}=3.6(V), L_1=L_2=L_3=L_4=230μH and C_1=C_2=0.66μF with 0.01ohm ESR, respectively. The switching frequency was 16.67 KHz and the duty ratio was D=0.53 for both $V_{B1}>V_{B2}>V_{B3}$ and $V_{B1}<V_{B2}<V_{B3}$ to ensure that the proposed bi-directional dc-to-dc converter could be designed to operate in DCVM. This can obtain a zero voltage switching (ZVS) to reduce the MOSFET switching loss in the proposed ICEs.

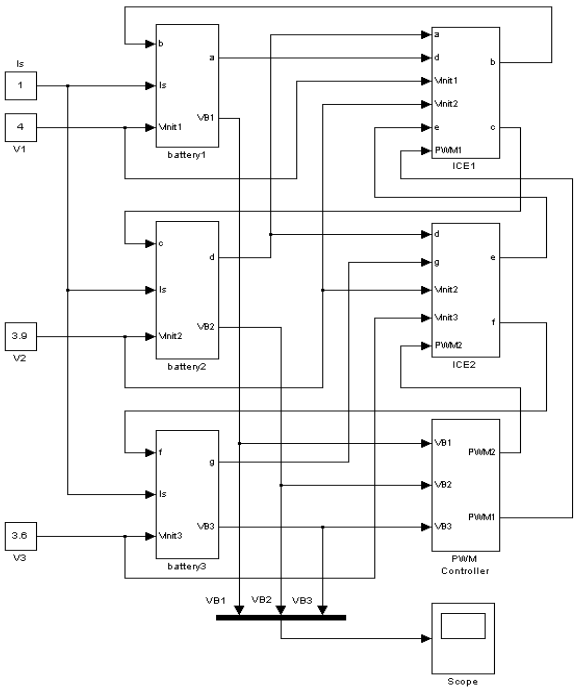

Fig. 7 Configuration of MATLAB/SimuLink model

Figure 8 shows the simulation voltages and currents for the capacitor and inductor in ICE1, respectively. The MOSFET control signal V_{gs} and the corresponding drain-source voltage V_T for $V_{B1}>V_{B2}>V_{B3}$ are shown as figs. 9 (a) and 9 (c). The simulation results of the cell voltage trajectories under static state, added 1A charging and discharging current states of the proposed battery equalizer are illustrated an the figs. 10 (a), (c) and (e), respectively. The cell balancing process is stopped when the cell voltage is equalized to the same end-of-charge or end-of-discharge state.

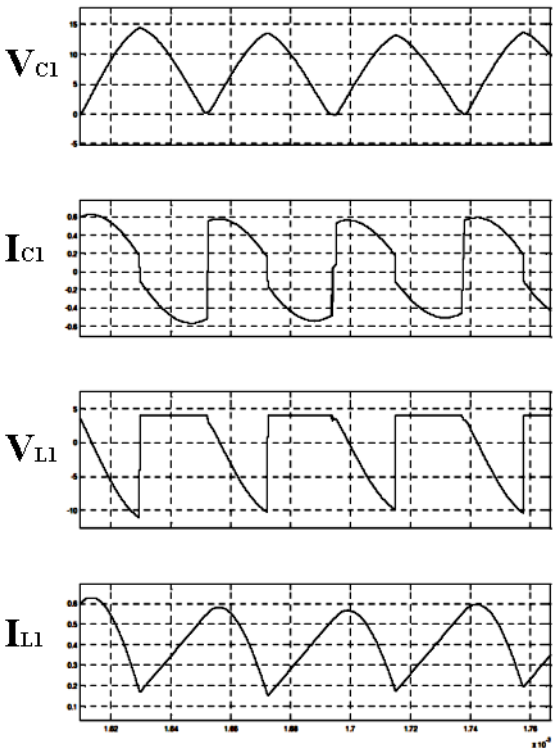

Fig. 8 Simulation results

The experimental installation of a three-modular lithium ion battery stack with the proposed equalization scheme is used to verify the equalization performance of the three cells battery stack with the proposed ICEs. The driving signals for the equalization schemes are controlled using a microprocessor-based battery management system according to each cell voltage. The driving signals are constructed using a logical switching algorithm, and instructed by processor of AT89C52.

Cell voltages were balanced within 0.0196 (V), due to the hardware resolution, which was limited by the analogue to digital converter (ADC0804). The voltage balancing process is stopped when the BMS sends an executable command to cut off the MOSFET. The experimental parameters of the batteries and the designed ICEs are listed as follows: The initial voltages of the three lithium-ion batteries MRL/ITRT 10AH are 4.0 (V), 3.5 (V), and 3.0 (V), respectively. The inductances are L_1~L_4=230μH, C_1=C_2=0.66μF. The switching frequency and the duty ratio of the battery equalizer are 16.67 kHz and 0.53, respectively. Figs. 9 (b) and 9 (d) show the measured voltages of V_{gs}, V_c, and MOSFET drain-source voltage V_T, respectively. The transient oscillations in the drain-source voltage of MOSFET due to the fast switching transient effect can be suppressed by well designed turned off DRC snubber circuits in the switching devices. Figs 10 (b), (d) and (f) show the experimental results of the cell voltage trajectories under static, added 1A charging and discharging current states of the proposed battery equalizers. Therefore, the equalization method can balance all the adjoining cell voltages of the battery string to the same voltage level. Consequently, each cell can be simultaneously charged to the end-of-charge voltage, so the total charging capacity of the battery string would be increased.

Figure 12 shows the equalization efficiency of ICE under various operating modes for the specified equalization processing. Figure 11 shows the waveform and the corresponding FFT spectrum of MOSFET switch power P_T (= $V_T * i_T$). Table 1 shows the differential designed results and performance comparison of the ICEs operated at CICM, DICM and DCVM under the specified equalization procession and equalizing current, respectively. Several observations on the proposed battery equalizer can be summarized as follows:

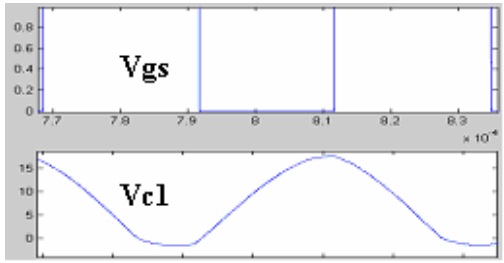

9. (a)

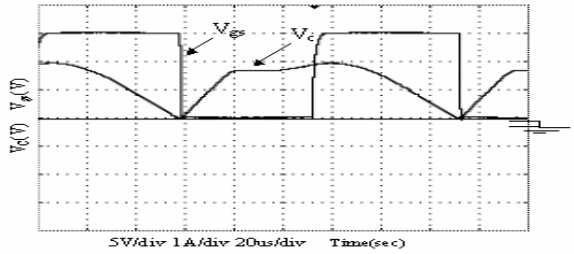

9. (b)

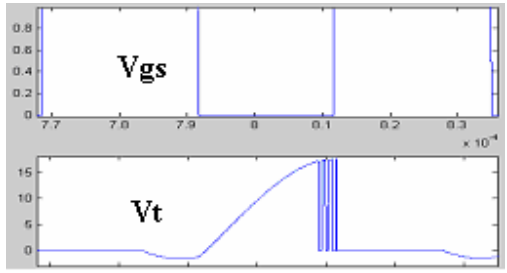

9. (c)

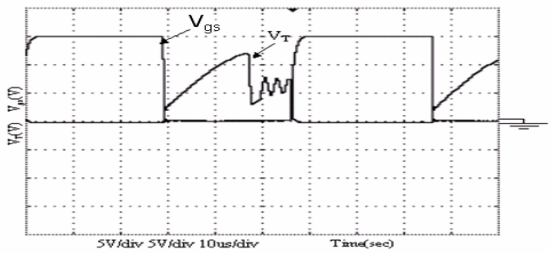

9. (d)

Fig. 9 Simulation and experimental results of MOSFET control signal V_{gs} and drain-source voltage V_T for V_{B1}>V_{B2}>V_{B3}, (a)(c) Simulations, (b)(d) Experiments

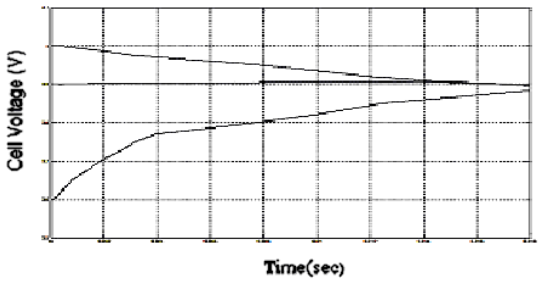

10. (a) Simulation

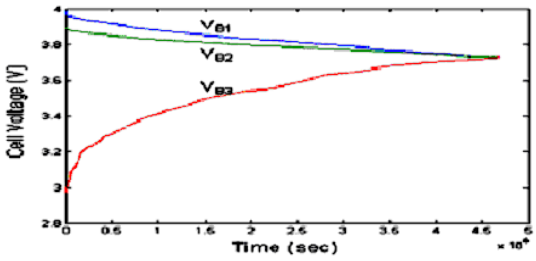

10. (b) Experiment

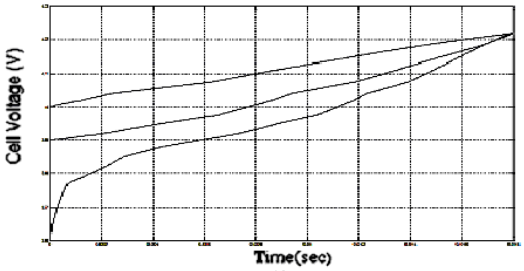

10. (c) Simulation

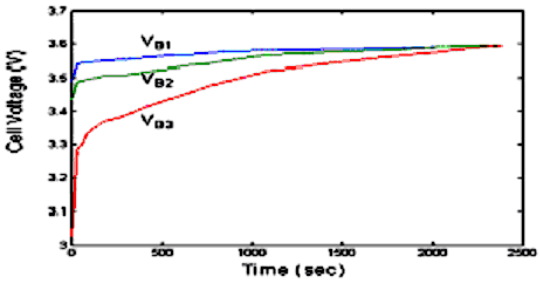

10. (d) Experiment

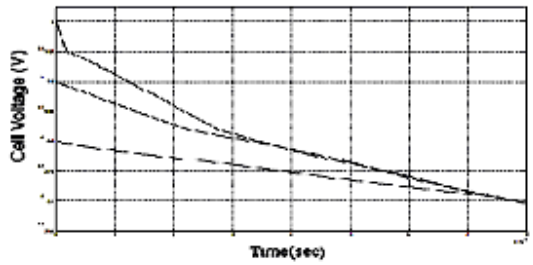

10. (e) Simulation

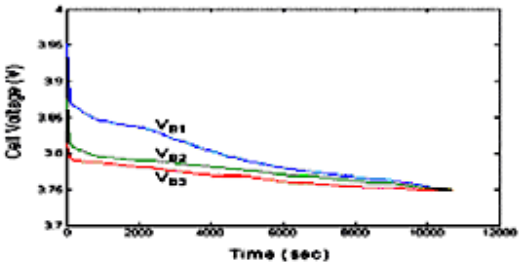

10. (f) Experiment

Fig. 10 Simulation and experimental results of cell voltage trajectories for $V_{B1}>V_{B2}>V_{B3}$, (a) (b) static state, (c) (d) added 1A charging current, (e) (f) added 1A discharging current

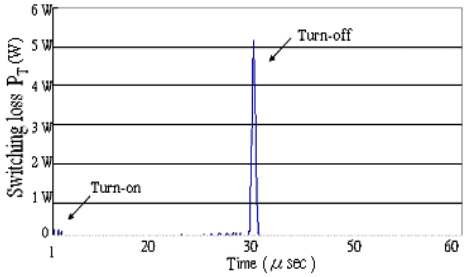

11. (a)

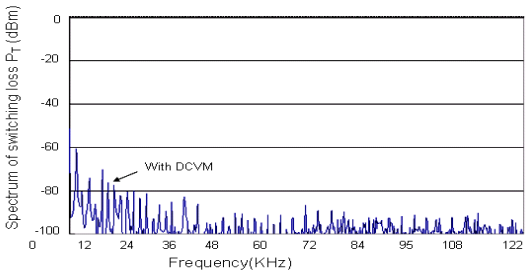

11. (b)

Fig. 11 (a) Waveform and, (b) FFT spectrum of MOSFET switch power

- The power MOSFETs of the proposed battery equalizer are turned off in the zero voltage state. The total switch power of the MOSFETs in the battery equalizer can be significantly reduced from 33.5% to 52.8% compared with the same equalizer operated at CICM (D=0.53).
- The peak current stress of the MOSFET is significantly reduced compared with the equalizer designed to operate at DICM (D=0.5).
- The average equalization efficiency can be improved from 52% to 68% compared with the equalizer operated at CICM. The maximum equalization efficiency of 72% can achieved for this designed test sample.
- The DCVM ZVS Cûk converter has spent slight more equalization time to balance the cell voltage to equal end-of-charge state. Therefore, it is necessary to design an equalization controller to speed up the equalization processing for a smart battery management system.

V. CONCLUSION

An ICE for the ZVS soft-switching of DC/DC converter has been proposed. To implement the zero-voltage-switching technique that can greatly reduce the power loss. The proposed ICE's MOSFET is turned off and the body diode is turned on at zero voltage of capacitor in DCVM. When the capacitor voltage approaches zero then the body diode of MOSFET is turned on until the capacitor energy is completely transferred to the weaker cell of batteries. Therefore, the MOSFET switch power is reduced by about 52.8% more than in CICM. The MOSFET switch power and the corresponding FFT frequency spectrums of the proposed battery equalizer in the DVCM are less than that in the DICM and CICM. The energy harmonic spectrum is concentrated in the low frequency for CICM, and is dispersed low to higher frequency in DCVM. Hence, the high frequency EMI emission is improved in a series-connected battery energy system with DCVM designed ICEs.

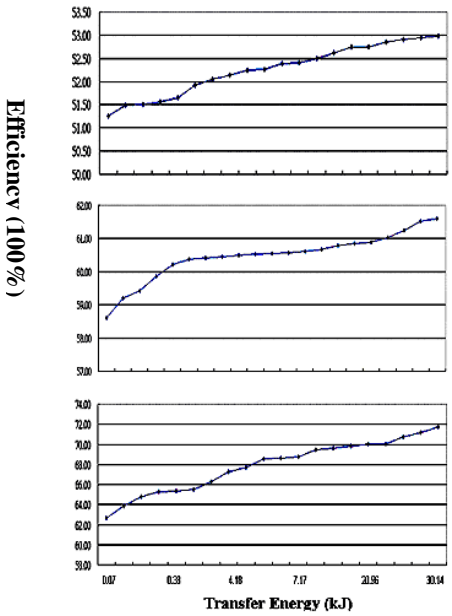

Fig. 12 Equalization efficiency of ICE under various operating modes

TABLE 1 COMPARISON BETWEEN CONTINUOUS AND DISCONTINUOUS MODES

	CICM	DICM	DCVM
Inductor (L_j)	99.1u	99.1u	231.2u
Inductor (L_{j+1})	100.7u	100.7u	231.2u
Capacitor(C_j)	470u	470u	0.66u
Switching frequency(f_s)	18.1K	16.67K	16.67K
Duty cycle (D)	0.53	0.5	0.53
Boundary condition for CICM and DICM	$L_j \cdot f_s > \frac{V_+(1-D)}{2I_+}$ $L_j \cdot f_s > \frac{(1-D)^2 \cdot V_+}{2D \cdot I_+}$	$L_j \cdot f_s < \frac{V_+(1-D)}{2I_+}$ $L_j \cdot f_s < \frac{(1-D)^2 \cdot V_+}{2D \cdot I_+}$	
Boundary condition for CICM and DMV	$D < \sqrt{2 \cdot \frac{V_+}{I_+} f_s C_j}$		$D > \sqrt{2 \cdot \frac{V_+}{I_+} f_s C_j}$
Voltage stress	Low	Low	High
Current stress	Low	High	Low
Switching characteristic	*	Soft turn-on	Soft turn-off
Most appropriate applications	*	Low current, high voltage	High current, low voltage

V. REFERENCES

[1]. H. V. Venkatasetty, and Y. U. Jeong," *Recent Advanced in Lithium-Ion and Lithium-Polymer Batteries,*" Proceeding of Battery Conference on Applications and Advances, The Seventeenth Annual, Jan. 2002, pp. 173-178.

[2]. J. McDowell, A. Brenier, M. Broussely, and P. Lavaur," *Industrial Lithium-Ion Batteries: From The Laboratory to Real Telecom Application,*" Proceeding of Telecommunications Energy Conference, INTELEC 24th Annual International, Sept. 2002, pp. 373-378.

[3]. N. H. Kutkut," *A Modular Nondissipative Current Diverter for EV Battery Charge Equalization,*" Proceeding of Applied Power Electronics Conference and Exposition, APEC'98, Thirteenth Annual, Vol. 2, 1998, pp 686 -690.

[4]. K. Nishijima, H. Sakamoto, and K. Harada," *A PWM Controlled Simple and High Performance Battery Balancing System,*" Proceeding of IEEE Power Electronics Specialists Conference, PESC'00, IEEE 31st Annual, Vol. 1, 2000, pp 517 -520.

[5]. Z. Zhang, and S. Cûk," *A High Efficiency 1.8 kW Battery Equalizer,*" Proceeding of IEEE Applied Power Electronics Conference and Exposition, APEC '93, Eighth Annual, 1993, pp 221 –227.

[6]. S. W. Moore and G. Maclean," *Control and Management Strategies for The Delphi High Power Lithium Battery,*" Proceeding of The 18th International Battery, Hybrid and Fuel Cell Electric Vehicle Symposium & Exhibition, EVS18 Berlin, 2001.A4B.

[7]. W. F. Bentley," *Cell Balancing Considerations for Lithium-Ion Battery Systems,*" Proceeding of the 1997 Battery Conference on Applications and Advances, Twelfth Annual, 14-17, Jane, 1997, pp.223-226.

[8]. S. W. Moore, and P. J. Schneider," *A Review of Cell Equalization Methods for Lithium Ion and Lithium Polymer Battery Systems,*" SAE Technical Paper Series, 2001-01-0959, March, 5-8, 2001, pp.1-5.

[9]. Y. S. Lee and C. W. Jao," *Fuzzy Controlled Lithium-Ion Battery Equalization with State-of-Charge Estimator,*" Proceeding of 2003 IEEE International Conference on System, Man and Cybernetics, IEEE CSMC2003, pp. 4431-4438.

[10]. J. Chatzakis, K. Kalaitzakis, N. C. Voulgaris, and S. N. Manlas," *Designing A New Generalized Battery Management System,*" IEEE Transaction on Industrial Electronics, Vol. 50, No. 5, 2003, pp.990-999.

[11]. Y. S. Lee and M. W. Cheng," *Intelligent Control Battery Equalization for Series Connected Lithium-Ion Battery Strings,*" Accepted and to be appearance in IEEE Transactions on Industrial Electronics.

[12]. P. Melin and O. Castillo," *Intelligent Control of Complex Electrochemical System with A Neuro-Fuzzy-Genetic Approach,*" IEEE Transaction on Industrial Electronics, Vol. 48, No. 5, 2001, pp. 951-955.

[13]. D. Maksimovic and S. Cûk," *A Unified Analysis of PWM Converters in Discontinuous Modes,*" IEEE Transactions on Power Electronics, Vol.6 No.3, July 1991, pp.476 –490.

[14]. M. Brkovic and S. Cûk," *Automatic Current Shaper with Fast Output Regulation and Soft-Switching,*" Telecom Energy Conference, INTELEC'93, 15th International Conference, Vol. 1, Sept. 1993, pp. 379-386.